Adhesion-Induced Domain Formation by Interplay of Long-Range Repulsion and Short-Range Attraction Force: A Model Membrane Study

A. Albersdörfer,* T. Feder,# and E. Sackmann*
*Biophysics Laboratory, Physics Department, Technische Universität München, D-85747 Garching, Germany, and #Physics Today, College Park, Maryland 20740 USA

ABSTRACT We study the role of the interplay of specific and universal forces for the adhesion of giant vesicles on solid supported membranes. To model the situation of cell adhesion, we incorporated lipopolymers (phospholipids with polyethyleneoxide headgroups) as artificial glycocalix, whereas attractive lock-and-key forces are mimicked by incorporating biotinylated lipids into both membranes and by mediating the strong coupling through streptavidin. Adhesion is studied by quantitative reflection interference contrast microscopy (RICM), which enables visualization of the contact zone and reconstruction of the height profile of the membrane beyond the contact line (outside the contact zone) up to a height of 1 μm. We demonstrate that adhesion is accompanied by lateral phase separation, leading to the formation of domains of tight adhesion (adhesion plaques) separated by areas of weak adhesion exhibiting pronounced flickering. By analyzing the height profile $S(x)$ near the contact line in terms of the tension equilibrium (Young equation) and the moment equilibrium, respectively, the adhesion energy and membrane tension can be approximately measured locally. We show that the adhesion energy is about three orders of magnitude larger for the adhesion plaques than for the weakly adhering regions. The adhesion is studied as a function of the excess area of the vesicle generated by temperature variation. A very remarkable finding is that increased excess area is not always stored in the contact area, but leads to the formation of microbuds (diameter $\approx$ 2 μm).

INTRODUCTION

The adhesion of cells is controlled not only by a complex interplay of specific lock-and-key forces and universal forces, but also by the elasticity of the plasma membrane and the shape of the soft shell (Bell, 1978; Bruinsma, 1995; Evans, 1985; Lipowsky and Seifert, 1991; Leckband et al., 1995; Seifert and Lipowsky, 1990). One distinct feature of many mobile cells is the formation of local sites of tight adhesion (so-called adhesion plaques), which is associated with receptor aggregation. By the attachment of actin bundles extending through the cytoplasm to the inner membrane leaflet at the adhesion plaques, cells may strongly adhere to substrates and may simultaneously minimize the loss of membrane material (for instance, during locomotion, when the trailing ends detach from the substrates). The adhesion sites are believed to be formed by the local segregation of receptors, which is expected to be associated with the concomitant lateral displacement of carriers of the glycocalix, to reduce the local repulsion between the opposing membranes, which is required for the formation of tight adhesion plaques (Ammann and Lipowsky, 1996).

To explore the opposing interplay between short-range attraction and medium- to long-range repulsion caused by the interpenetration of the glycocalices of the opposing membranes and by the undulation forces, respectively, we studied the interaction between giant vesicles and supported membranes on solid supports. In our model system the glycocalix is mimicked by incorporation of lipopolymers (polyethyleneoxide-substituted phosphatidylethanolamine, abbreviated as PEO-lipid) into membranes. The short-range attractive forces are realized by phospholipids with biotin-carrying headgroups and by using streptavidin as a strong connector.

To facilitate the settlement of the giant vesicles onto the substrate, they were filled with a slightly denser aqueous solution than the suspension medium. The excess area of the vesicles was controlled by temperature variations to study the effect of shape changes on the adhesion.

The adhesion of the vesicles is evaluated by quantitative reflection interference contrast microscopy (RICM). Analysis of the surface profile of the vesicles near the contact line enables measurements of the contact angle ϑ_c and the contact curvature R_c^{-1}. By considering the balance of tensions (Young equation) and bending moments at the contact line, respectively, the adhesion-induced membrane tension and the adhesion energy can be measured locally. This enables separate measurements of the adhesion energies at the adhesion domains (pinning centers) and at the regimes determined by steric and undulation forces.

We demonstrate that the contact formation of flaccid vesicles with the supported membrane is followed by the rapid appearance of local sites of close contacts, which are separated by regimes whose adhesion is controlled by undulation forces. At low receptor concentrations (<0.1 mol%), the strong adhesion domains remain separated for hours, whereas at higher concentrations (>1 mol%) they merge to form a single patch within minutes.

Received for publication 2 December 1996 and in final form 19 March 1997.

Address reprint requests to Dr. Erich Sackmann, Biophysics Laboratory, Physics Department E22, Technische Universität München, James-Franck-Strasse, D-85747 Garching, Germany. Tel.: 49-89-2891-2472; Fax: 49-89-2891-2469; E-mail: sackmann@physik.tu-muenchen.de.

0006-3495/97/07/245/13 $2.00

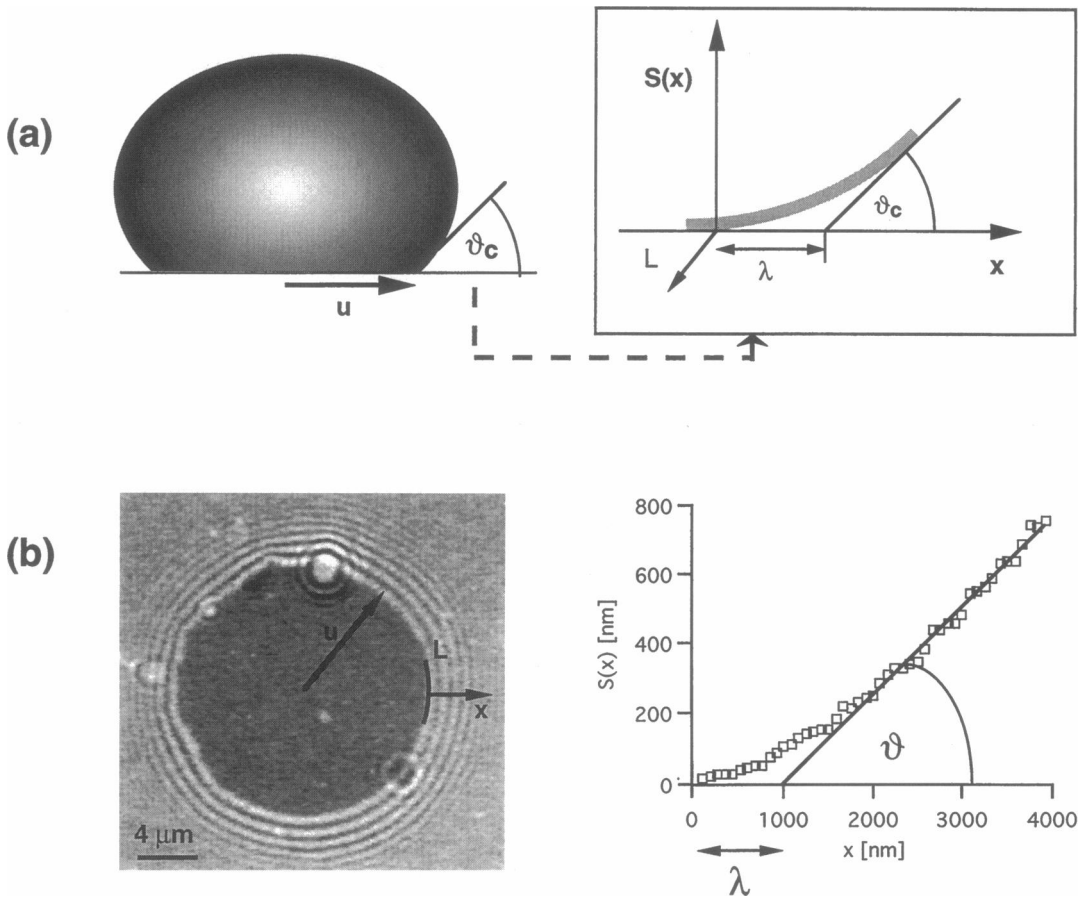

FIGURE 1 (*a*) Schematic view of an adhering vesicle for definition of geometric parameters. The radius u of the adhesion disk and the contact angle ϑ between vesicle and surface are defined through a linear extrapolation of the vesicle surface far from the edge down to the substrate. R' is the vesicle radius in the state of adhesion. The insert shows an enlarged view of the rim of the adhesion disk in which the vesicle surface $S(x)$ starts to curve away from the substrate. L is the contact line, and λ is the width of the rim as defined in the text. (*b*) *Left*: RICM micrograph of an adhering vesicle. The vesicle radius was measured simultaneously by transmission light microscopy (the result is not shown in this picture). *Right*: Contour of the vesicle near contact line as obtained by analyzing the interference pattern of the RICM micrograph. The width of the rim λ and the contact angle J are obtained by analyzing the contact contour perpendicular to L in terms of a straight line, and a locally curved region, at the contact line.

Surprisingly, we often found a sudden decrease in the contact area when increasing the excess area of the vesicle shell. This is attributed to the spontaneous formation of microbuds competing with the adhesion.

THEORETICAL BACKGROUND OF CONTOUR ANALYSIS

The adhesion strength of vesicles can be analyzed in two ways: first, by a rigorous method based on the analysis of the vesicle shape as a function of the ratio of vesicle area to volume, the adhesion energy and the membrane tension; and second, by analyzing the contour of the vesicle near the substrate in terms of the mechanical equilibrium at the contact line of the adhering vesicle. The former approach can be applied only for isotropic adhering shells, and the latter is best suited for evaluating the present RICM experiments. In particular, it enables local approximations of adhesion energies and tensions.

The mechanical equilibrium of weakly adhering shells with smooth contact lines is determined to a first approximation by the equilibrium of the lateral tension within the fluid membrane and of the bending moment at the boundary. The equilibrium of tension is determined by Young's law:

$$W = \sum(1 - \cos \vartheta_c) \tag{1}$$

where W is the adhesion energy per unit area (or the membrane-substrate interfacial energy), Σ is the lateral tension, and ϑ_c is the contact angle defined in Fig. 1.

The bending moment of a soft shell fixed at a contact area is related to the bending stiffness κ and the curvature $\partial^2 S/\partial n^2|_c$ in a direction, $\vec{n}$, perpendicular to the contact line L (Landau and Lifschitz, 1986).

$$M = \kappa \left.\frac{\partial^2 S}{\partial n^2}\right|_c \tag{2}$$

The bending moment can be related to the adhesion energy W by considering the work $= M\partial^2 S/\partial n^2\ \delta n$ performed by the bending moment to displace the contact line by a distance δn in a direction normal to L. Because this work is equal to the change in adhesion energy ($2W\delta n$), and because $M = \kappa\partial^2 S/\partial n^2|_c$, one obtains

$$2W = \kappa\left(\frac{\partial^2 S}{\partial n^2}\right)^2 \tag{3}$$

where the factor 2 accounts for the fact that two surfaces are formed during the displacement of the membrane from the surface.

The moment equilibrium prevents the formation of a sharp edge of the adhering shell at the contact line. As pointed out by Bruinsma (1995), this corresponds to a line tension, because the bending moment tends to pull the adhering shell away from the substrate at the contact line.

In principle, adhesion energies can be obtained by measuring the contact curvature R_c^{-1} by evaluation of the surface profile $S(\vec{r})$ near the contact line and by application of Eq. 3. This procedure enables only order-of-magnitude measurements of R_c. A more accurate method is suggested by a recent, simplified model of the adhesion of soft shells by Bruinsma (1995) that can be applied for weak adhesion if the surface profile near the substrate is dominated by membrane tension. In the limit of small contact angles ($\vartheta_c \leq 20°$), we can write for the local contact angle (Bruinsma, 1995; Landau and Lifschitz, 1986)

$$\vartheta = \left.\frac{\partial S(r)}{\partial r}\right|_c \cong \frac{u}{R} \tag{4}$$

where $S(\vec{r})$ is the surface profile perpendicular to the contact line L, u is the radius of the contact zone, and R is the vesicle radius. The Young equation (1) yields

$$\frac{1}{2}\vartheta^2 \cong \frac{W}{\Sigma} \tag{5}$$

The adhesion-induced change of the free elastic energy can be expressed in terms of the relative strain u/R as

$$\Delta G_{adh} = \pi W u^2 + 2\pi u\tau + \frac{1}{4}\pi\Sigma R^2\left(\frac{u}{R}\right)^4 + \frac{\pi}{128}ER^2\left(\frac{u}{R}\right)^8 \tag{6}$$

where E is the Young modulus. The last two terms account for the adhesion-induced extension and for the bending outside of the rim of the contact line, respectively. The bending energy at the transition from the adhering to the free membrane is accounted for by introduction of the line tension τ (second term on the right side). The gain in adhesion energy is represented by the first term.

The radius, u, of the adhesion disk can in principle be determined by minimizing the free energy with respect to u. The behavior is largely determined by the line tension τ. If the bending at the rim is neglected ($\tau = 0$), ΔG_{adh} exhibits a single minimum at $u/R = \vartheta = \sqrt{2W/\Sigma}$, which is Young's law. For $\tau \neq 0$, ΔG_{adh} is a cubic equation exhibiting two minima, and Eq. 6 thus predicts a first-order transition at a critical value of τ,

$$\tau_c^2 = \frac{4}{27}W^3R^2/\Sigma \tag{7}$$

In the present work we are concerned with the surface profile near the contact zone. Following the method of Bruinsma (1995), this profile can be calculated by considering a straight contact line, L, and then minimizing the elastic energy perpendicular to L (in the direction x):

$$\Delta G = 2\pi u\left[\int_0^\infty dx\left\{\frac{1}{2}\kappa\left(\frac{d^2S}{dx^2}\right)^2 + \frac{1}{2}\Sigma\left(\frac{dS}{dx}\right)^2\right\} - \int_{-\infty}^0 W(x)dx\right] \tag{8}$$

The height profile $S(x)$ near the rim is thus determined by the differential equation

$$\Sigma\frac{d^2S}{dx^2} - \kappa\frac{d^4S}{dx^4} = 0 \tag{9}$$

For large x the profile $S(x)$ must be linear: $S(x) = \vartheta x - \vartheta\lambda$, whereas for $x = 0$ (position of the contact line), $S(x) = 0$.

A solution satisfying these boundary conditions is (cf. Fig. 1)

$$\begin{aligned} S(x) &= \vartheta x - \vartheta\lambda\left[1 - \exp\left(-\frac{x}{\lambda}\right)\right] && (x > 0) \\ S(x) &= 0 && (x \leq 0) \end{aligned} \tag{10}$$

where according to Eq. 9, $\lambda = \sqrt{\kappa/\Sigma}$ is a characteristic length scale that is a measure for the range over which the surface profile is determined by bending elasticity. According to Eq. 3, λ is related to the contact curvature by $\lambda = \vartheta_c R_c$.

The above considerations hold for straight or smoothly curved contact lines; for sharply curved contact lines one also has to consider the boundary condition for the force equilibrium, which is of the form (Landau and Lifschitz, 1986)

$$f = \kappa\left(\frac{\partial^3 S(r)}{\partial x^3} + \Sigma\rho_c^{-1}(r)\frac{\partial^2 S(r)}{\partial x^2}\right) \tag{11}$$

where ρ_c^{-1} is the curvature of the contact line. Therefore, the surface profile can be analyzed by Eq. 10 alone if the curvature of the contact line is small compared to the curvature of the surface profile ($\rho_c^{-1} \ll \partial^2 S/\partial x^2$).

MATERIALS AND METHODS

Vesicle preparation

Vesicles were prepared by swelling in an electric field as described by Rädler and Sackmann (1993). We used dioleoylphosphatidylcholine (DOPC); dioleoylphosphatidylethanolamine-polyethyleneoxide (DOPE-PEO_{2000}), with a headgroup composed of 45 monomers corresponding to a molecular mass of 2000 Da, and biotin-X-dioleoylphosphatidylethano-

lamine (DOPE-X-biotin), a lipid with a biotin linked to the headgroup via a 10–15-Å hydrocarbon spacer. All lipids were purchased from Avanti Polar Lipids (Birmingham, AL). Mixtures of 5 mol% DOPE-PEO_{2000} and various amounts of DOPC and DOPE-X-biotin were dissolved in chloroform. Then, 150 μl of the lipid stock solution was spread onto indium tin oxide (ITO)-coated coverslips (Balzers, Liechtenstein) and dried in a vacuum chamber for 12 h. After desiccation, the coverslips were placed in a sucrose solution, and vesicles were swollen in an AC field of 18 V/cm, at 10 Hz, which was applied for 1 h at 40°C.

We first ascertained by phase-contrast microscopy that successful vesicle swelling had occurred. A typical sample contained vesicles of a wide range of sizes, some with diameters larger than 150 μm.

Substrate preparation

First monolayers of dimyristoyl phosphatidyl choline (DMPC) were deposited by the Langmuir-Blodgett technique onto glass coverslips that were coated with a 55-nm film of MgF_2 (refractive index $n = 1.386$) to increase the contrast (Rädler and Sackmann, 1993). The MgF_2 was vacuum deposited at 10^{-6} atm, 380°C substrate temperature, and 3 nm/s deposition rate. Bilayers were formed by horizontal dipping of the monolayer-covered sample through the monolayer on the air/water interface into the subphase and were continuously kept below water. The upper monolayer was composed of the same lipid mixture as the vesicle membranes. The transfer was done at a pressure π of 25 mN/m and at room temperature.

The coverslips carrying the supported membrane were mounted in a measuring chamber that allowed temperature control. The samples were incubated for 1 h with streptavidin at a concentration of 100 ng/ml (MoBiTec, Göttingen, Germany) in buffer (100 mM NaCl, 10 mM HEPES, pH 7). After the incubation the bulk solution was exchanged by rinsing the measuring chamber at least 10 times with pure buffer, so that only streptavidin molecules bound to biotin receptors within the supported membrane were left in the measuring chamber. Finally, the vesicles in suspension were added to the measuring chamber. The osmotic gradient was adjusted so that the vesicles were flaccid during the measurements.

Reflection interference contrast microscopy

We observed the contact zone of adhering vesicles by RICM and measured the circumference of the equator of the vesicles simultaneously by light microscopy. The measuring device as well as the method of quantitative analysis of the RICM images by image processing have been described previously (Rädler et al., 1995; Rädler and Sackmann, 1993). The interference pattern resulting from the interference of light reflected from the membrane and from the substrate, respectively, is evaluated as follows: to a first approximation, the measured intensity $I(x)$ at a lateral position x is related to the vertical membrane-substrate displacement $S(x)$ by

$$I(S(x)) = I_1 + I_2 + 2\sqrt{I_1 I_2}\cos[2kS(x) - \delta_1 + \delta_2] \qquad (12)$$

where $k = 2\pi n/\lambda$ denotes the wave vector, with n being the refraction index of the medium ($\lambda = 546.1$ nm, $n_{buffer} = 1.33$). I_i is the intensity and δ_i the corresponding phase shift of the light reflected from the ith surface. The distance $S(x)$ can be calculated from the measured intensities $I(x)$ according to

$$S(x) = \frac{\lambda}{4\pi n}\left[\arccos\left(\frac{2I(x) - (I_{max} + I_{min})}{(I_{max} - I_{min})}\right) + \delta_1 - \delta_2\right] \qquad (13)$$

I_1, I_2 are expressed here in terms of the measurable quantities I_{min} and I_{max}.

As shown by Rädler and Sackmann (1993), a 55-nm film of MgF_2 (corresponding to a $\lambda/8$ optical path length) on the coverglass enhances the contrast. In addition, the MgF_2 film leads to a monotone increase in the intensity if the membrane-substrate distance varies within the range of $0 < S < 100$ nm.

At the rim of the adhering region, the vesicle membrane begins to curve away from the substrate and the membrane-substrate distance $S(x)$ eventually exceeds 100 nm. Above this limit the interference pattern exhibits extrema that correspond to higher order fringes. Under the assumption that the membrane bends monotonically away from the surface, these extrema can be used to determine the edge contour of the adhering vesicle. The extrema are related to the heights by (Rädler et al., 1995; Rädler and Sackmann, 1993)

$$S_j = j\frac{\lambda}{4n} + \arccos(\delta_1 - \delta_2) \qquad (14)$$

where j is an integral number and δ_1 and δ_2 are defined in Eq. 12.

RESULTS AND DISCUSSION

Formation of patches

Fig. 2 shows a RICM micrograph of a supported bilayer containing 94 mol% DOPC, 5 mol% DOPE-PEO_{2000}, and 1 mol% DOPE-X-biotin before and after incubation with streptavidin. The bright domains that occur after the incubation are attributed to two-dimensional protein crystals, as reported earlier for streptavidin molecules bound to biotinylated monolayers (Blankenburg et al., 1989; Darst et al., 1991). These domains are surrounded by regions of lower streptavidin density.

Additional lateral diffusion measurements by fluorescence recovery after photobleaching of the bound streptavidin molecules (not shown in this paper) showed that the lateral diffusion of the bound connectors in the supported bilayer is suppressed.

In Fig. 3, a vesicle adhering to the streptavidin-coated supported membrane described above is shown. The vesicle membrane was of the same composition as the substrate membrane. The area of contact and the decoupled contour up to a height of ~1 μm are visible. The top row and the picture at the bottom left are snapshots taken at time intervals of ~0.1 s and clearly demonstrate strong flickering of the vesicle. Closer inspection shows some apparently stationary dark regions, which are attributed to pinning centers. To check this conclusion, 64 images recorded at a time interval of 0.1 s were averaged. The average image shown in Fig. 3 (*bottom right*) demonstrates that five dark patches of close contact are formed. The patches were stable over hours.

The interpretation of the dark patches as domains of tight adhesion is further strengthened by determining the profile of the distance $S(x)$ between the vesicle surface and the substrate near the edges of the patches. This can be done by directly analyzing the averaged intensity values using Eq. 13. Fig. 4 *a* shows as an example a time-averaged micrograph of an adhering vesicle and a three-dimensional plot of the averaged distance about an adhesion domain in terms of gray values between the adhesion patch and the environment.

A more effective method of analysis is based on the measurement of the mean square fluctuations $\langle|S(t)_x - \langle S(t)\rangle_x|^2\rangle$ of the height near the rim of the strong adhesion patch. This analysis also yields insight into the profile of the dynamic surface roughness near the patches. Fig. 4 *b* shows

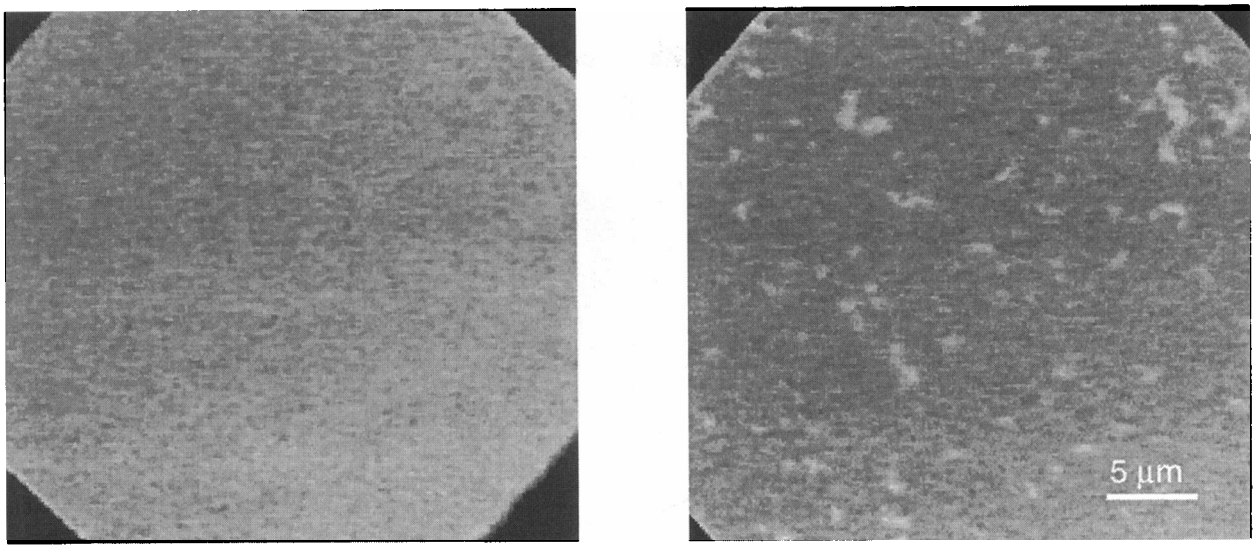

FIGURE 2 RICM micrograph of a supported bilayer containing 94 mol% DOPC, 5 mol% DOPE-PEO_{2000}, and 1 mol% DOPE-X-biotin in the upper layer. (*a*) Bilayer before incubation with streptavidin. (*b*) Bilayer after incubation with streptavidin (1 nM for 1 h). The streptavidin molecules, bound to the biotin receptors in the supported bilayer, exhibit a phase separation in streptavidin-rich domains, which appear as bright clusters and areas of lower streptavidin concentration.

three plots of the long wavelength height fluctuations (as obtained from the fluctuations of the gray values) as a function of time at sites 1, 2, and 3 indicated in Fig. 4 *a*. The short wavelength fluctuations make only an insignificant contribution and are averaged out, owing to the finite integration time of the camera.

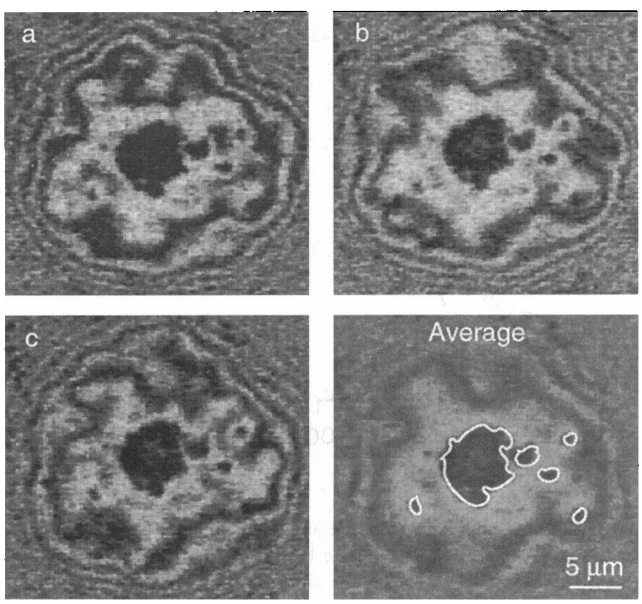

FIGURE 3 RICM micrograph of an adhering giant vesicle containing 94 mol% DOPC, 5 mol% DOPE-PEO_{2000}, and 1 mol% of biotinylated lipid in the vesicle membrane. The streptavidin-coated supported membrane was of the same composition as in Fig. 2. Three snapshots (*a*, *b*, and *c*) and the average over 64 images (*bottom right*) are shown. The local sites of close contact between vesicle and substrate are outlined in white.

Following the method of Helfrich (Helfrich, 1978; Helfrich and Servuss, 1984), we calculate the vertical roughness amplitude:

$$\xi_\perp(x) = \sqrt{\langle |S(t)_x - \langle S(t)\rangle_x|^2\rangle} \tag{15}$$

which is related to the mean separation distance $\langle S(x)\rangle$ by

$$\xi_\perp(x) = c_\perp \langle S(x)\rangle \tag{16}$$

where $c_\perp$ is a dimensionless constant that has been determined by Monte Carlo calculations to be $c_\perp \approx 0.445$ (Lipowsky, 1994). The resulting separation distance profile $S(x)$ is shown in Fig. 4 *c*. Starting at the pinning center, where the separation distance is zero within experimental error, the membrane curves away from the surface.

This method is applicable only near the patches within 100 nm of the surface where the intensity fluctuations do not reach the maximum possible value. If this limit is exceeded, the gray value analysis does not yield unique values of the distance fluctuations, because of the ambiguity of the arc cosine function in Eq. 13. In particular, the determination of the absolute separation distance in the regime of weak adhesion is not possible, because of this ambiguity. However, even the variation of the separation distance near the edge of the patches demonstrates the difference between local sites of close contact and more distant regimes of adhesion controlled by undulation forces.

Formation and growth of adhesion patches

Fig. 5 *a* shows the time evolution of the size of the adhesion plaques. The process starts with the nucleation of patches that appear immediately after the first contact between vesicle and substrate. This nucleation process is followed by

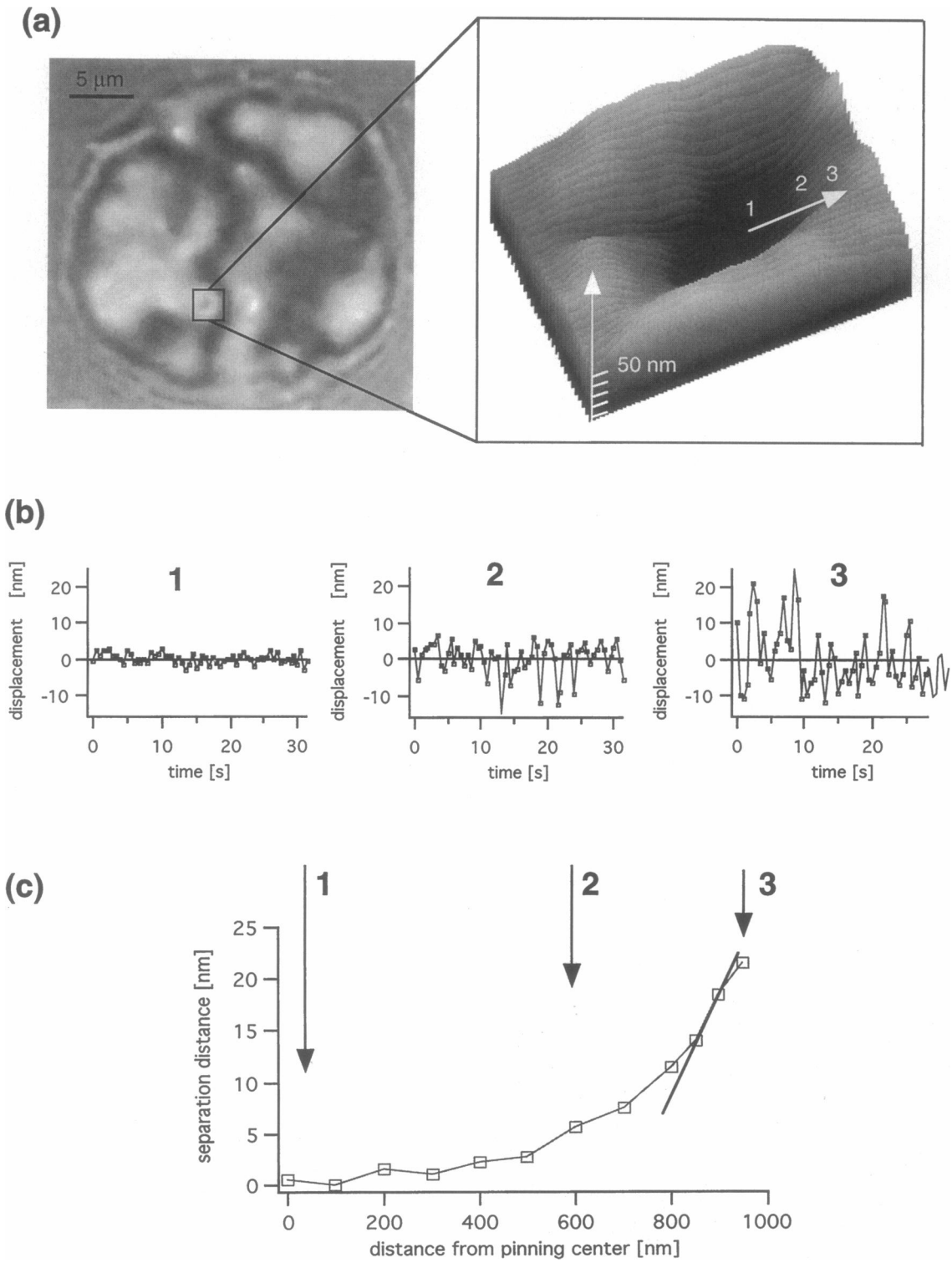

FIGURE 4 (*a*) *Left*: Time-averaged RICM micrograph of an adhering vesicle. The two opposing membranes are composed of 95 mol% DOPC, 5 mol% DOPE-PEO_{2000}, and 0.1 mol% DOPE-X-biotin. The right side shows a three-dimensional plot of the approximate height above the surface (about the encircled pinning center visible on the micrograph) expressed in terms of gray values. The height was calculated by applying Eq. 12. (*b*) Plot of temporal fluctuations of the membrane displacement caused by thermal undulations at the positions marked by numbers 1, 2, and 3 in *a*. (*c*) Separation distance between vesicle membrane and substrate along the line shown in *a* (*right side*). The average separation distance was calculated from the height fluctuations. At a distance between 10 nm and 20 nm, a slope of the separation distance dS/dx of ~ 0.04 was determined, which corresponds to a bending modulus of $\kappa \approx 10^{-19}$ J.

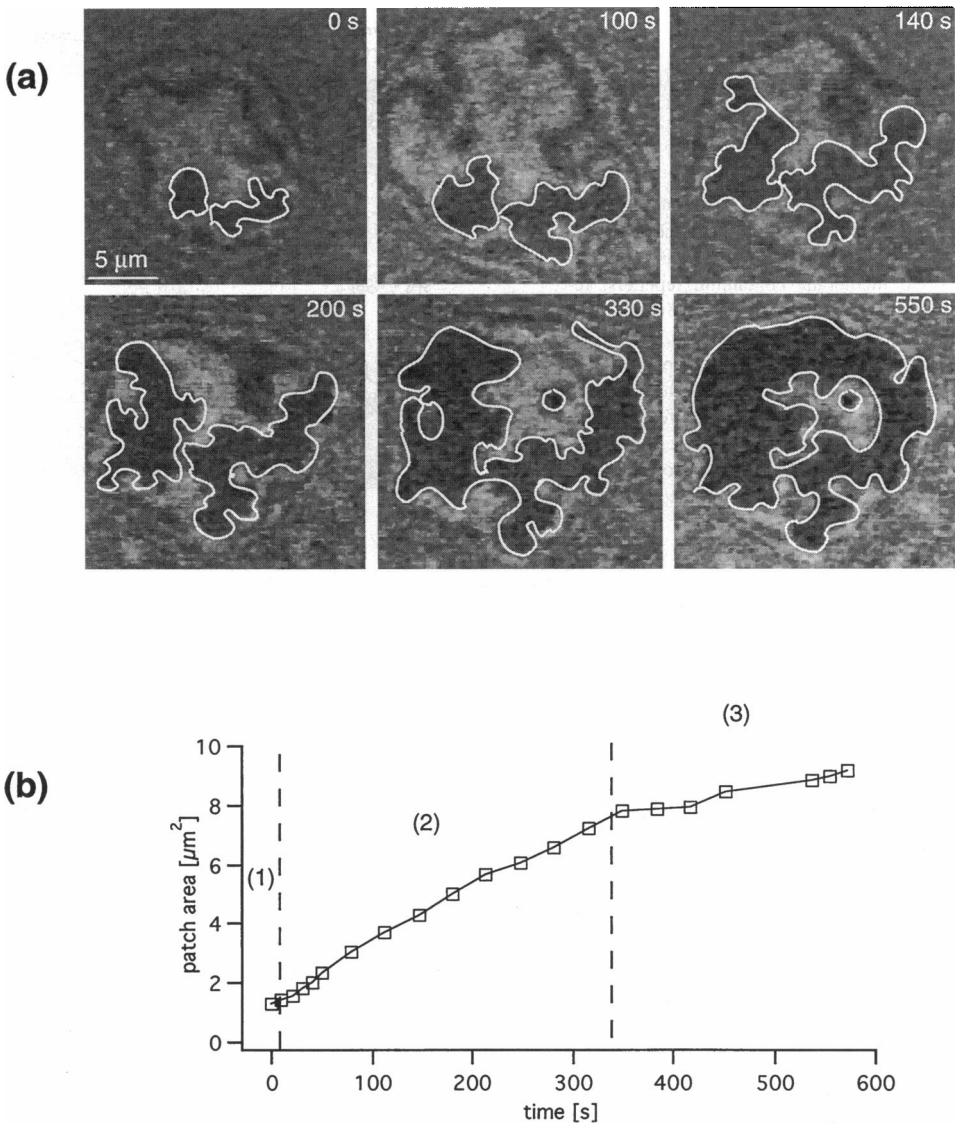

FIGURE 5 (*a*) Time evolution of adhesion plaques for a vesicle adhering to a streptavidin-coated supported membrane. The two opposing membranes are composed of 94 mol% DOPC, 5 mol% DOPE-PEO_{2000}, and 1 mol% DOPE-X-biotin. The adhesion plaques are outlined in white. The vesicle radius was measured simultaneously with an additional light microscope (not shown in this picture). (*b*) The total area of the adhesion patches is plotted as a function of time. Three regimes marked by vertical lines are observed: *(1)* A spontaneous initial formation of adhesion plaques, *(2)* a regime of fast growth, and *(3)* a slowing down behavior of the patch growth, which results in saturation of the tight contact area.

the growth of the plaques along the edges of the contact zone of the vesicle, eventually followed by fusion of the plaques. The last stages of growth are characterized by a very slow increase in the plaque area, accompanied by an increase in the average diameter of the ringlike patch. Interestingly, a small patch that developed at $t \approx 350$ s in the middle of the contact zone stops growing after being encircled by the outer patch.

The time evolution of patch growth is shown in more detail in Fig. 5 *b*. The total area of the adhesion plaques was determined by analyzing 21 images and is plotted as a function of time. As described above, we find three patterns of behavior: 1) the spontaneous formation of small adhesion domains by nucleation, 2) fast growth of the plaques, and 3) a slowing down of the patch growth, resulting in the saturation of the tight contact area.

The spontaneous patch formation is attributed to local segregation of receptors, which is accompanied by lateral displacement of the lipopolymers to reduce the local repulsion between the opposing membranes. The adhesion plaque formation is shown schematically in Fig. 6. The data in Fig. 5 *b* can be interpreted in terms of a diffusion-controlled process, as suggested by Noppl-Simson and Needham (1996). The biotin receptors, attached to freely mobile lipid molecules in the vesicle membrane, diffuse into the contact zone from the surrounding vesicle membrane. Because the streptavidin molecules in the supported membrane are immobile, the biotin receptors are immobilized as soon as they reach an already formed adhesion domain. This is responsible for the preferred growth of the adhesion plaques at the rim of the contact zone. However, we cannot exclude the possibility that attractive interactions between the receptors are the major driving forces for the receptor clustering (Lipowsky, 1996).

If we assume that this process is diffusion limited, the average time required for the completion of the patch formation is on the order of $\tau_D \approx 2D_B R^2$, where R is the radius of the vesicle, D_B is the diffusion coefficient of the biotin

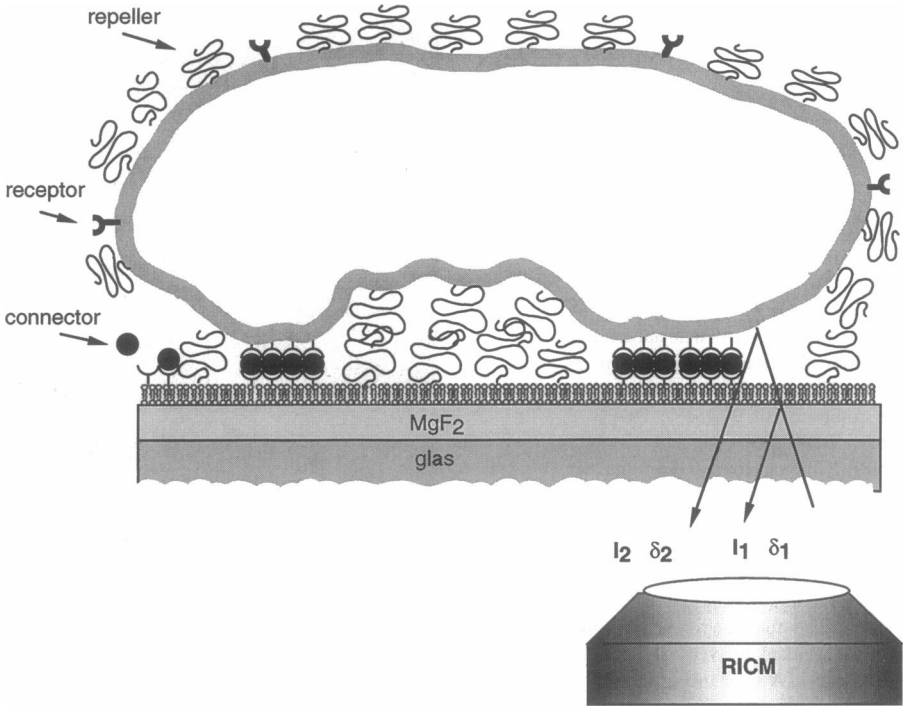

FIGURE 6 Schematic view of a vesicle composed of repellers (lipopolymers) and receptors (biotinylated lipid) adhering to a supported membrane containing repellers, receptors, and connectors (streptavidin). The polymer and biotin headgroups, which are located at the inner side of the vesicle membrane, are not depicted. Also shown is the principle used in reflection interference contrast microscopy: the images are formed by interference of light reflected from the substrate (I_1) and from the vesicle membrane (I_2), respectively.

lipid, and τ_D is the characteristic diffusion time. In the case of Fig. 5, the vesicle radius is $R \approx 20$ μm and $\tau_D \approx 200$ s. This corresponds to a value of $D_B \approx 2$ $\mu m^2/s$, which is in good agreement with the diffusion coefficients measured for phospholipids.

In contrast to the in vivo situation, where the membrane components of both bilayers are free to diffuse, the dynamic process of adhesion plaque formation in our experiments is only determined by the receptors in the vesicle membrane. This is due to the fact that one bilayer is supported on a solid surface and its receptors are immobilized.

The saturation of the total area of adhesion plaques in our experiments is a result of the limited amount of biotin receptors available in the vesicle. The patch formation shown in Fig. 5 reveals a second process occurring when a nearly closed ring of tight contact has been formed. The ringlike patch forms a barrier for the biotin lipids, leading to a strongly reduced diffusion and slowing of the patch growth rate. This behavior is equivalent to that of a percolation process.

Adhesion energy of pinning centers

Fig. 7 *a* shows the contact zone of a vesicle containing 5 mol% of lipopolymers but only 0.1 mol% biotin receptors adhering to a supported membrane of the same composition. In contrast to the vesicles presented in Figs. 3 and 5, only small adhesion plaques are formed. The diffraction fringes are remarkably distorted near the pinning centers, as shown by closer inspection of position 4 in Fig. 7 *a*. As shown in the following, the distortion is a consequence of the higher tension and of the increased adhesion energy.

By application of the simplified model described in the theoretical section, we may estimate the local tension and adhesion energy by analyzing the intensity profiles perpendicular to the contact line along the sections marked in Fig. 7 *a* by white bars. Three examples of these contours are shown in Fig. 7 *b*: one in the region of a pinning center (position 4d), one in a region which is not influenced by a pinning center (position 8), and one that lies somewhere between these two regions (position 4g).

Following Bruinsma (1995), the curves may be analyzed in terms of a straight-line regime far away from the contact line and a more curved regime upon approaching the edge of the contact zone. By extrapolation of the straight lines to the abscissa, one obtains the values λ and ϑ, defined in Eq. 10. From these values we determined the tension Σ_{local} and the adhesion energy W_{local}. In some cases contact curvatures R_c were fitted to the curves. The values thus obtained agree within a factor of 2 with the values obtained from λ as described above. For these calculations we used a value of $\kappa \approx 35\ k_BT$ for the bending modulus, which was measured for pure SOPC (stearoyl phosphatidyl choline) vesicles by other techniques (Duwe and Sackmann, 1990; Evans and Parsegian, 1983). The results are listed in Table 1 and plotted in Fig. 7 *c*.

A remarkable behavior is found at the center of the pinning center (position 4d). The slope of the straight-line regime near the contact line is rather steep (resulting in a small value of λ), but then the slope relaxes back to the value corresponding to that of the weakly adhering regime (e.g., position 8). This behavior clearly shows that the contact curvature is much smaller at position 8 than at position 4d. According to Eq. 1, this corresponds to a larger

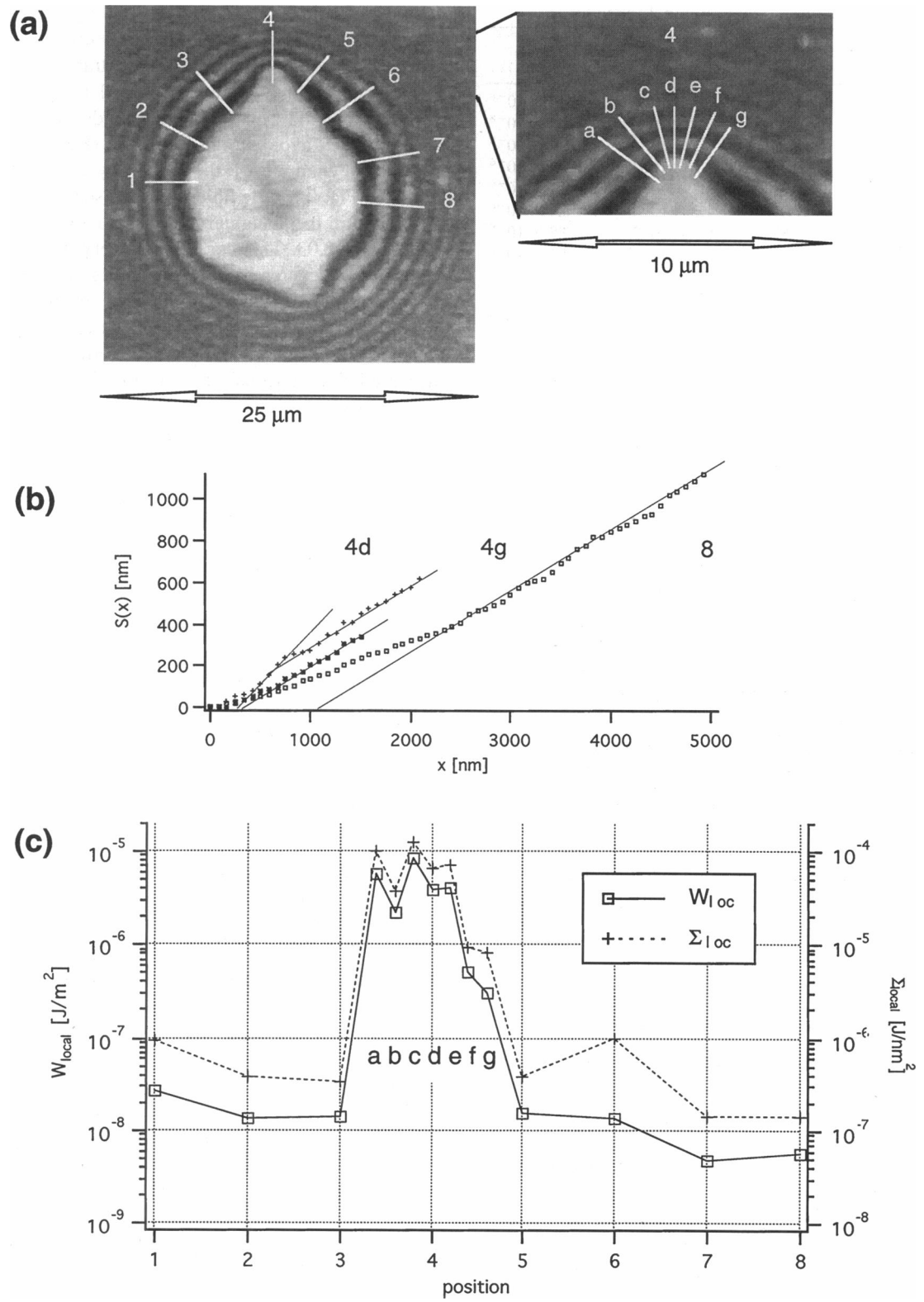

FIGURE 7 (*a*) Time-averaged RICM micrograph of the contact zone of an adhering vesicle composed of 94.9 mol% DOPC, 5 mol% DOPE-PEO_{2000}, and 0.1 mol% DOPE-X-biotin. The streptavidin-coated supported membrane was of the same composition as the vesicle membrane. (*Inset*) Enlarged view of the upper section with the pinning center. The white bars mark the directions along which contact contours are analyzed. (*b*) Three examples of contours near contact area: one in the region of a pinning center (position 4d), one in a region that is not influenced by a pinning center (position 8), and one that is situated in between these two regions (position 4g). (*c*) Local tensions (*dashed line*) and adhesion energies (*drawn line*) plotted versus the position line number marked in *a*.

TABLE 1 Parameters and calculated local tensions

Position	λ (nm)	ϑ (deg)	Σ_{local} (J/m^2)	W_{local} (J/m^2)
1	400	13.7°	9.3×10^{-7}	2.7×10^{-8}
2	632	15.3°	3.8×10^{-7}	1.3×10^{-8}
3	670	16.5°	3.3×10^{-7}	1.4×10^{-8}
4a	38	18.9°	1×10^{-4}	5.7×10^{-6}
4b	63	20.1°	3.8×10^{-5}	2.3×10^{-6}
4c	35	21.3°	1.2×10^{-4}	8.4×10^{-6}
4d	48	19.8°	6.5×10^{-5}	3.9×10^{-6}
4e	46	19.3°	7.1×10^{-5}	4.1×10^{-6}
4f	126	18.8°	9.5×10^{-6}	5.1×10^{-7}
4g	135	15.6°	8.3×10^{-6}	3×10^{-7}
5	627	16.7°	3.8×10^{-7}	1.5×10^{-8}
6	395	9.7°	9.6×10^{-7}	1.4×10^{-8}
7	1032	15.0°	1.4×10^{-7}	4.8×10^{-9}
8	1039	16.2°	1.4×10^{-7}	5.7×10^{-9}

First two columns: parameters λ and ϑ defined in Eq. 1 and 10 as obtained by analyzing the contours along the directions marked in Fig. 7. The last two columns show the calculated local tensions S_{local} and adhesion energies W_{local}.

adhesion energy of the adhesion plaque. Our analysis shows that the local adhesion energy at a pinning center is more than two orders of magnitude larger then typical values far away from such a center (cf. Table 1). The same holds for the tension.

The distortion of the interference fringes near the pinning centers is due to the deformation of the membrane surface by the increase in adhesion strength. This behavior is very similar to the deformation of the surface of adhering liquid drops near pinning centers predicted by Joanny and de Gennes (1984). The only difference is that in the present case, the distortion of the contour is determined by both tension and bending moment, which leads to a change in the logarithmic law for the force generated by the pinning centers. We shall discuss this point in more detail in a forthcoming paper.

Competition between wetting and budding

Another remarkable finding is shown in Fig. 8, where the size of the contact area is studied as a function of the excess area generated by thermal expansion of the membrane through heating from 298 K to 304 K. (The excess area is the difference between the actual area and that which would be required to form a sphere of the same volume.)

One would intuitively expect that a monotonous increase in the excess area should lead to a concomitant increase in the contact area. Surprisingly, the contact area decreases after the excess area is increased, typically by $\sim 200\ \mu m^2$ (Fig. 8 *b*). This is attributed to a competition between budding and increasing adhesion area during expansion of the bilayer.

First, a strong reduction in the long-wavelength flickering amplitudes is caused during the drop in contact area, as is expected if the excess area is stored in the small buds (Häckl and Sackmann, unpublished data). This is more directly demonstrated in Fig. 8 *a*, where the long-wavelength fluctuations of the flicker amplitudes are recorded as a function of time before and after the budding transition.

Second, the long-chain lipids used here have a strong tendency toward formation of microbuds during area expansion, and they avoid strong flickering (Käs and Sackmann, 1991). An example of this tendency toward budding is shown in Fig. 9 for the lipid mixture used here. The ratio of the areas of the daughter vesicles to that of the mother vesicle is ~ 0.03. This corresponds very well with the two drops in contact area by 200 μm^2 in Fig. 8 *b* for a vesicle of $A_0 = 6900\ \mu m^2$. Reductions in area of similar size have indeed been observed repeatedly. The approximate vesicle area was calculated from the vesicle radius, which has been measured simultaneously by transmission light microscopy as mentioned above.

In the regions between the budding transitions the vesicle shows a roughly linear increase in the contact area with the temperature (Fig. 8 *b*), and the slope is nearly the same before and after the region of instability. From this we may determine the thermal area expansivity coefficient of our vesicles according to

$$\alpha = \frac{1}{A_0}\frac{dA_c}{dT} \tag{17}$$

where A_0 is the area of the vesicle and A_c the contact area. Using the data from our experiments, we obtain $\alpha \approx 6.6 \times 10^{-3}\ K^{-1}$. The result agrees reasonably well with the values of α measured previously for other PC vesicles ($\alpha_{DMPC} \approx 7.3 \times 10^{-3}\ K^{-1}$, $\alpha_{POPC} \approx 3.5 \times 10^{-3}\ K^{-1}$; Käs and Sackmann, 1991).

GENERAL DISCUSSION

Patch formation by local phase separation and the influence of undulation forces

The present work shows that the formation of adhesion domains is a natural consequence of the competition between short-range attraction and long-range repulsion. To form a site of close contact, work must be performed against the repulsion forces. As pointed out by Bruinsma et al. (1994), this results in attraction between the points of close contact. In the present case, the repulsion between vesicle and substrate is strongly determined by polymer-induced forces (exhibiting a range of $\sim 2 \times 3.5$ nm) and undulation forces.

The average thickness of the headgroup of the lipopolymer in the mushroom configuration (which is the most likely configuration in our experiments) is ~ 3.5 nm, which is roughly equal to the distance of the center of the connecting streptavidin molecules from the membrane surface. One therefore expects that the formation of tight contacts is also driven to some extent by local phase separation, resulting in the squeezing out of lipopolymers (repellers) from the adhesion domains. Although the phase separation in the contact area of the vesicle is accompanied by a decrease in

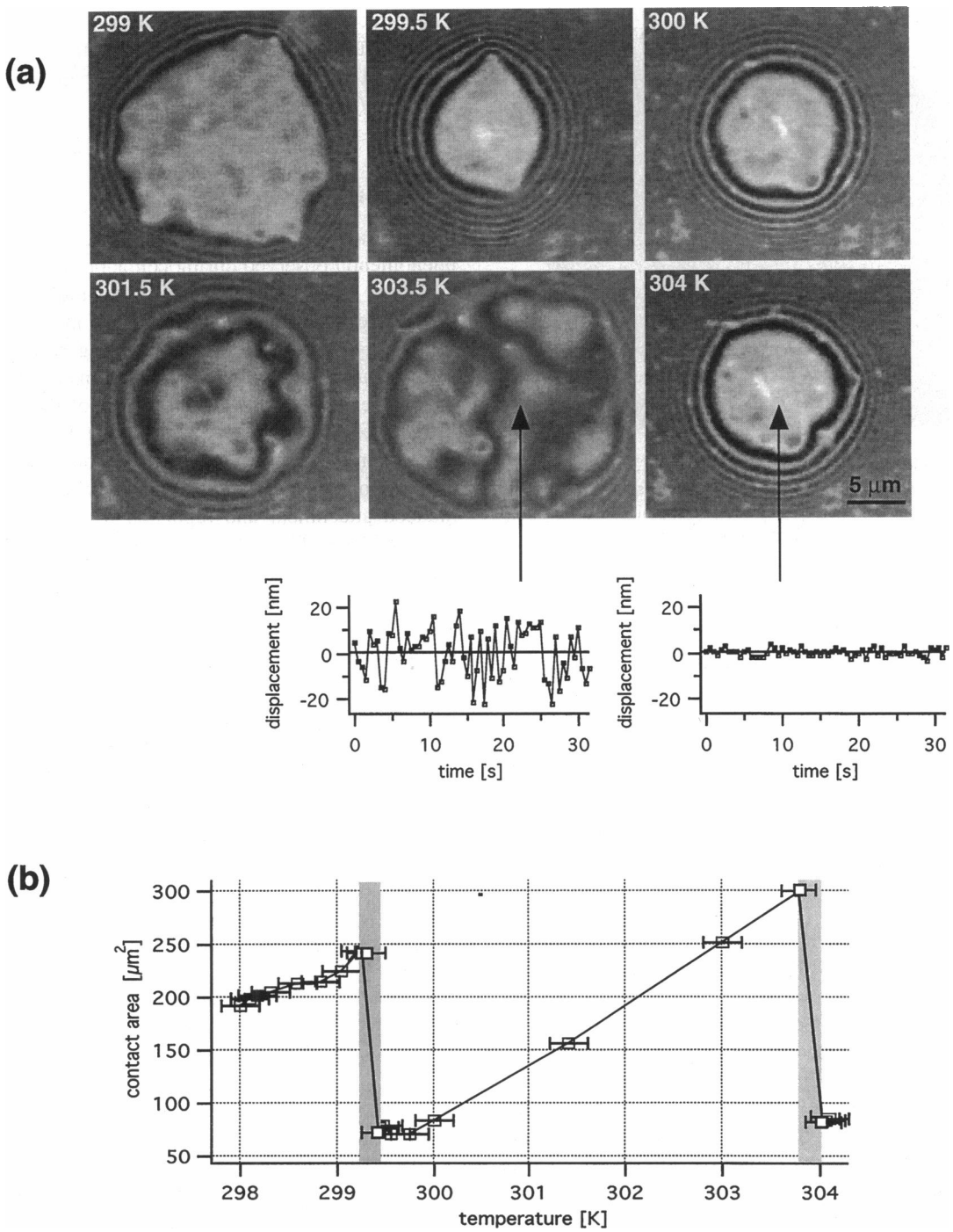

FIGURE 8 (*a*) Change of the contact area of an adhering vesicle composed of 94.9 mol% DOPC, 5 mol% DOPE-PEO_{2000}, and 0.1 mol% DOPE-X-biotin on a streptavidin-coated supported membrane of the same composition, caused by increasing the excess area of the vesicle by increasing the temperature from 298 K to 304 K. Note the sudden drops in contact area between 299 and 299.5 K and between 303.5 and 304 K. The traces at the bottom show plots of temporal fluctuations of the distance between vesicle and support for a situation immediately before and after the drop in contact area. (*b*) Plot of contact area as a function of temperature. The regions marked by gray bars emphasize the sudden decrease in the contact area.

entropy, a net decrease in free energy can result if the repulsive potential is great enough.

In the weakly adhering region separating the pinning centers (where the separation distance exceeds 7 nm), the distance between vesicle membrane and substrate is determined by undulation forces. Following Bruinsma et al. (1994), the average height profile $S(x)$ near circular pinning centers should follow a linear law,

$$S(r) \approx \sqrt{k_B T/\kappa^* r} \tag{18}$$

From Fig. 4 *c* we can determine the slope of the height profile and estimate the bending modulus by assuming the

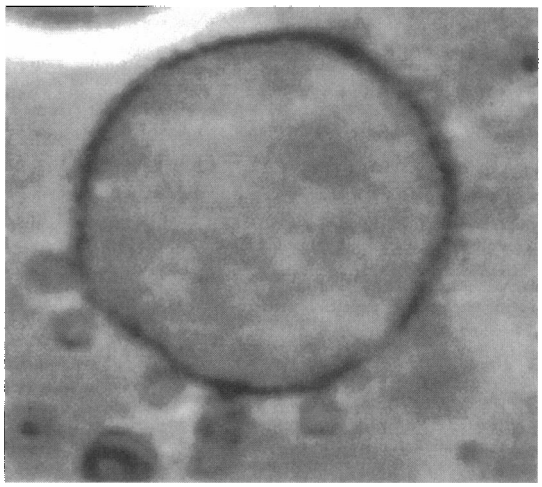

FIGURE 9 Vesicle composed of 94.9 mol% DOPC, 5 mol% DOPE-PEO_{2000}, and 0.1 mol% DOPE-X-biotin, taken with phase-contrast microscopy, showing several adjacent microbuds. These exhibit a rather sharp size distribution, with an average diameter of ~5 μm.

above equation. At a distance between 10 nm and 20 nm, where the repulsion is only determined by undulation forces, the slope of the separation distance dS/dx is ~0.04, which yields a value of $\kappa \approx 10^{-19}$ J. This is in good agreement with the bending modulus measured by other techniques (Duwe and Sackmann, 1990).

Concerning evolution of adhesion plaques

The formation of adhesion plaques starts with the formation of nuclei of close contact. These grow by diffusive transport of free biotin-lipids from the whole outer monolayer. At high concentrations of "receptors," the growing plaques merge, resulting in slowing of the growth. The formation of the adhesion plaques in the present case is essentially irreversible because of the high binding energy of the streptavidin-biotin bond, which is ~34 k_BT (Green, 1975), and the high energy of the biotin-lipid binding in the membrane, which is ~30 k_BT (Evans, 1985; Evans et al., 1992; Chiruvolu et al., 1994; Bell, 1978; Cevc and Marsh, 1987). Despite this equality of the binding energies, separation is expected to occur by pulling out the biotin-lipid from the bilayer for the following reason.

The force required to separate bonds is determined by the binding energy divided by the distance over which the molecules must be moved to break the bonds. This distance is ~2 nm for pulling the lipid out of the bilayer and ~0.5 nm for separating the biotin-streptavidin bond. The force required to pull out the lipid is thus smaller by factor of 5 than the force required to break the biotin-connector bond. But it is strong enough to prevent the detachment of the bonds over the time scale of hours. The small domains found in the case of low receptor concentrations are therefore in a frozen-in state and do not merge.

The receptor density in the domains of tight adhesion is expected to be determined by the streptavidin density in the supported bilayer, which is $\sim 10^{16}$ m^{-2} in the case of dense covering (Green, 1975).

Biological implications

The formation of local centers of attachment is a common phenomenon observed during cell adhesion. It enables cells to adhere strongly to substrates and simultaneously allows them to detach again at minimal loss of membrane materials.

The aggregates of strongly adhering receptors (such as integrins in the case of fibroplasts) form centers from which stress fibers extend toward the center of the cell.

The present experiments suggest that the driving force for the formation of adhesion plaques could be the receptor aggregation due to the competition between strong receptor-induced attachment and repulsion forces. Up to now, no clear evidence for a dominant contribution of undulation forces to this repulsion has been found, and it may well be that in the case of cells the repulsion is determined by the glycocalix. Some evidence for this view is provided by the finding that adhesion plaques are also formed by vinculin-deficient cells (Goldmann et al., 1996). Vinculin, together with talin, is generally assumed to be essential for the formation of adhesion plaques and stress fibers. Interestingly, the plaques are broader in the case of wild-type cells.

REFERENCES

Ammann, A., and R. Lipowsky. 1996. Discontinuous phase transitions of membranes: a Monte Carlo study. *J. Phys. II France.* 6:255–270.

Bell, G. I. 1978. Models for the specific adhesion of cells to cells. *Science.* 200:618–627.

Blankenburg, R., P. Meller, H. Ringsdorf, and C. Salesse. 1989. Interaction between biotin lipids and streptavidin in monolayers: formation in oriented two-dimensional protein domains induced by surface recognition. *Biochemistry.* 28:8214–8221.

Bruinsma, R. 1995. Adhesion and rolling of leukocytes: a physical model. *Proc. NATO Adv. Inst. Phys. Biomater. NATO ASI Ser.* 332:61–75.

Bruinsma, R., M. Goulian, and P. Pincus. 1994. Self-assembly of membrane junctions. *Biophys. J.* 67:746–750.

Cevc, G., and D. Marsh. 1987. Phospholipid Bilayers: Physical Principles and Methods. John Wiley and Sons, New York.

Chiruvolu, S., S. Walker, J. Israelachvilli, F. J. Schmitt, D. Leckband, and J. A. Zasadzinski. 1994. Higher order self-assembly of vesicles by site-specific binding. *Science.* 264:1753–1757.

Darst, S. A., M. Ahlers, P. Meller, E. W. Kubalek, R. Blankenburg, H. O. Ribi, H. Ringsdorf, and R. D. Kornberg. 1991. Two-dimensional crystals of streptavidin on biotinylated lipid layers and their interaction with biotinylated macromolecules. *Biophys. J.* 59:387–396.

Duwe, H. P., and E. Sackmann. 1990. Binding elasticity and thermal excitations of lipid bilayer vesicles: modulation by solutes. *Physica A.* 163:410–428.

Evans, E. 1985. Detailed mechanics of membrane-membrane adhesion and separation. I. Continuum of molecular cross-bridges. *Biophys. J.* 48: 175–183.

Evans, E., D. Berk, and A. Leung. 1992. Detachment of aggulin-bonded red blood cells. I. Forces to rupture molecular-point attachments. *Biophys. J.* 59:838–848.

Evans, E., and V. A. Parsegian. 1983. Energetics of membrane deformation and adhesion in cell and vesicle aggregation. *Ann. N.Y. Acad. Sci.* 416:13–33.

Goldmann, W. H., R. M. Ezzell, E. D. Adamson, V. Niggli, and G. Isenberg. 1996. Vinculin, talin and focal adhesion. *J. Muscle Res. Cell Motil.* 17:1–5.

Green, M. 1975. Avidin. *Adv. Protein Chem.* 29:85–133.

Helfrich, W. 1978. Steric Interaction of fluid membranes in multilayer-systems. *Z. Naturforsch.* 33a:305–315.

Helfrich, W., and R. M. Servuss. 1984. Undulations, steric interactions and cohesion of fluid membranes. *Il Nuovo Cim.* 3D(1):137–151.

Joanny, J. F., and P. G. de Gennes. 1984. A model for contact angle hysteresis. *J. Chem. Phys.* 81:552–562.

Käs, J., and E. Sackmann. 1991. Shape transitions and shape stability of giant phospholipid vesicles in pure water induced by area-to-volume changes. *Biophys. J.* 60:825–844.

Käs, J., E. Sackmann, R. Podgornik, S. Svetina, and B. Zeks. 1993. Thermally induced budding of phospholipid vesicles—a discontinuous process. *J. Phys. II France.* 3:631–645.

Landau, L. D., and E. M. Lifschitz. 1986. Theory of Elasticity. Pergamon Press, New York.

Leckband, D. E., W. Müller, F. J. Schmitt, and H. Ringsdorf. 1995. Molecular mechanism determining the strength of receptor-mediated intermembrane adhesion. *Biophys. J.* 69:1162–1169.

Lipowsky, R. 1994. Generic interactions of flexible membranes. *In* Structure and Dynamics of Membranes, Vol. 1. R. Lipowsky and E. Sackmann, editors. Elsevier, Amsterdam. 554.

Lipowsky, R. 1996. Adhesion of membranes via anchored stickers. *Phys. Rev. Lett.* 77:1652–1655.

Lipowsky, R., and U. Seifert. 1991. Adhesion of vesicles and membranes. *Mol. Cryst. Liq. Cryst.* 202:17–25.

Noppl-Simson, D., and D. Needham. 1996. Avidin-biotin interactions at vesicle surfaces: adsorption and binding, cross-bridge formation, and lateral interactions. *Biophys. J.* 70:1391–1401.

Rädler, J., T. J. Feder, H. H. Strey, and E. Sackmann. 1995. Fluctuation analysis of tension-controlled undulation forces between giant vesicles and solid substrates. *Phys. Rev. E.* 51:4526–4536.

Rädler, J., and E. Sackmann. 1993. Imaging optical thickness and separation distances of phospholipid vesicles at solid surfaces. *J. Phys. II France.* 3:727–747.

Seifert, U., and R. Lipowsky. 1990. Adhesion of vesicles. *Phys. Rev. A.* 42:4768–4771.